DOI: 10.30511/pcdp.2026.2084569.1063 - ISSN: 3060-8376 - Vol 3(2), 2026

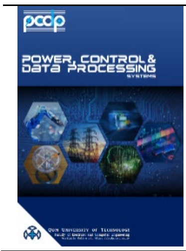

POWER, CONTROL AND DATA PROCESSING SYSTEMS

Available Online at: https://pcdp.qut.ac.ir/

Optimal Operation of Electricity and Hydrogen Integrated System with Fuel Cell Electric Vehicles and Uncertainties

ARTICLE INFO

Article Type
Original Research

Authors
Mohsen Bahmani[1]
Sina Ahmadi[1,*]
Mehrdad Setayesh Nazar[1]

[1] Department of Electrical Engineering
Shahid Beheshti University
Tehran, Iran

**** Correspondence***
Address: Department of Electrical Engineering
Shahid Beheshti University
Tehran, Iran
sina_ahmadi@Mail.sbu.ac.ir

mohsen_bahmani@Mail.sbu.ac.ir
sina_ahmadi@Mail.sbu.ac.ir
m_setayeshnazar@Mail.sbu.ac.ir

Article History
Received: February 04, 2026
Accepted: May 12, 2026
ePublished: June 01, 2026

ABSTRACT

The growth in renewable energies (REs) has created new challenges for balancing supply and demand, and for managing uncertainty in power systems. Integrated energy systems (IESs) based on hydrogen are a promising solution for increasing network resilience. This paper provides a daily optimization framework for electricity and hydrogen integrated system, which fuel cell electric vehicles (FCEV) not only as a consumer, but also as mobile storage resources. For accurate uncertainty modeling, a scenario generation method based on the Copula function has been used to maintain the correlation between random variables (solar radiation, wind speed, load, and energy price). Further, to reduce the computational burden, the scenarios have been reduced with the K-means optimization algorithm. The problem is formulated as mixed integer linear programming (MILP) to simultaneously minimize operating costs and environmental pollution. The numerical results show that implementing demand response reduced the peak-to-valley difference by 16.6%, 16.59%, and 22.5%, decreased operational costs by 10.2%, 7%, and 9.3%, and lowered environmental costs by 3%, 1.5%, and 4.48% across different seasons.

Keywords: Integrated energy system, Fuel cell electric vehicle, Uncertainty, Demand response.

1 Introduction

Today, energy systems are transitioning from fossil fuels to renewable energies (REs) to address the challenges of climate change and energy security. However, the intermittent and random nature of resources such as wind and solar has created new challenges in balancing supply and demand. To overcome this challenge, the concept of integrated energy systems (IESs) has been proposed, which increases the flexibility and efficiency of the system by connecting different energy carriers [1]. These systems allow the conversion of one energy into another energy and its storage. Ref [2] proposed an IES that includes a wind turbine (WT), photovoltaic (PV), electrolyzer (EL), fuel cell (FC), and hydrogen energy storage (HES), and solves a multi-objective problem for day-ahead. The results show a 3.5% reduction in carbon emissions with a slight increase in cost compared to the single-objective case. Fuel cell electric vehicles (FCEVs) are not considered in this study. Ref [3] presents a life cycle economic assessment method for wind-hydrogen integrated system, which analyzes the effects of the ratio of hydrogen production from wind and allocation to FC by calculating the payback period and net profit, and in the case study of a Chinese wind farm, reduces the payback from 11 to 8.13 years and increases the revenue from 670 to 930 million yuan. The scope of this study does not encompass FCEVs. Ref [4], the IES power-hydrogen scheduling model is introduced with power to heat and hydrogen (P2HH) and seasonal hydrogen storage technologies, and uncertainties are managed by stochastic and robust optimization to increase the stability of the system. Case studies demonstrate that the proposed model effectively optimizes equipment configuration. Hydrogen market is not considered in this study. Ref [5] proposes a two-level mixed integer linear programming (MILP) model for a regional power-hydrogen IES, where the first level optimizes the equipment configuration for energy demand, and the second level minimizes the normalized cost of hydrogen. The optimization results indicate that integrating hydrogen energy enhances operational flexibility. The study does not account for hydrogen exchange with the external market. Ref [6] integrates EL and hydrogen energy storage (HES) in IES with combined heat and power (CHP). The 24-hour MILP model shows a reduction in wind outages, fuel consumption, and carbon emissions. FCEVs are not considered in this study. Ref [7] offers a power-gas IES model with blending hydrogen. The simulation results based on real data illustrate the 36.5% reduction in gas. FCEVs are not modeled in this work. Ref [8] presents an assessment framework for future IES that covers multidimensional, multi-carrier, systemic, prospective, and applied features and considers interdependencies, as existing frameworks are inadequate. The results prove the feasibility of using natural gas network to absorb surplus renewable energy. FCEVs are not modeled in this work. Ref [9] presents a mixed integer non-linear programming (MINLP) model for a power-gas IES with HES that, with piecewise linearization, reduces operating costs by 5.96% and carbon emissions by 117.6 tons. FCEVs are not considered in this paper. Ref [10] formulized a operational model for power-hydrogen-heating IES with FC and El in connected and islanded modes, resolving uncertainties by correcting the management forecast error and by piecewise linearization and CPLEX. The results confirm the reduction of operating cost and improvement of reliability. The transaction with upper hydrogen market is not considered in this paper. Ref [11] proposed PV, photothermal, and photocatalysis oh hydrogen production based solar IES with radiation spectrum separation and component sizing method that satisfies the demand for electricity, heat and hydrogen and reduces the cost. The mathematical model for system component sizing is built. Ref [12] provide multi-career microgrid (MG) which including power, heat, cooling, gas, and hydrogen energies. The results indicate a reduction in operational cost. FCEVs are not considered in this model completely. Ref [13] presents a multi-objective model for optimizing energy hubs (EHs) and multi-energy networks with hydrogen, which manages uncertainties with Monte Carlo and solves with MILP to minimize annual cost and carbon emissions. The probable behavior of the FCEVs are not modeled. Ref [14] proposed a hybrid power-hydrogen storage configuration in IES with a discrete EH that, by reducing the K-means scenario, increases the consumption of REs to 98.873% and reduces the investment cost by 10%. FCEVs are not modeled in this work.

This paper presents a comprehensive framework for optimal daily scheduling of an integrated electricity and hydrogen system. The key objectives of this research are:

- Presenting an optimal operation model for an integrated electricity and hydrogen system, considering the active role of FCEV as a distributed generation source.
- Accurate modeling of the correlation framework between uncertainties of REs, load, and energy prices using a probabilistic approach based on the Copula function and scenario reduction with the K-means algorithm.
- Formulation of the problem as MILP with the aim of simultaneously minimizing operating costs and pollutant emissions and integrating demand response programs (DRPs).

In the following, section 2 describes the proposed method, section 3 presents the simulation results, and section 4 presents the conclusions.

2 Proposed method

In this paper, has developed a MILP model for daily operation of power-hydrogen IES. The main goal is to simultaneously minimize operating costs and pollutant emissions, taking into account uncertainties in the production of PV, WT, electrical load, and energy prices. The proposed model is solved in GAMS with the CPLEX solver. The schematic structure of the studied EHIES system is shown in Fig. (1). According to Fig. (1), the proposed EHIES consists of PV, WT, FC, EL, electrical energy storage (EES), and HES, which can convert input energy sources into various types of energy carriers for use, storage, or sale. Further, the connection between the electrical grid, hydrogen network, and FCEVs are considered. The input of EHIES includes electrical energy purchased from the upstream grid, FCEVs discharge, and also energy generated from PV and WT. The output of EHIES system also includes electrical and hydrogen energies.

The proposed system can exchange hydrogen and electrical energy with the FCEVs. An aggregator, which is the operator of the EHIES system, is responsible for scheduling the energy exchange with FCEVs. FCEVs enter the EHIES parking at a specific time and stay in the parking for many hours. When FCEVs are present in the parking, the parking operator is able to use FCEVs to generate electrical energy from hydrogen and send it into the grid. According to the results presented in Ref [46], which are based on experimental testing, FCEVs can inject electrical power into the grid with V2G capability. This work needs a separate V2G system, which is assumed to be available in the FCEV parking by the EHIES operator.

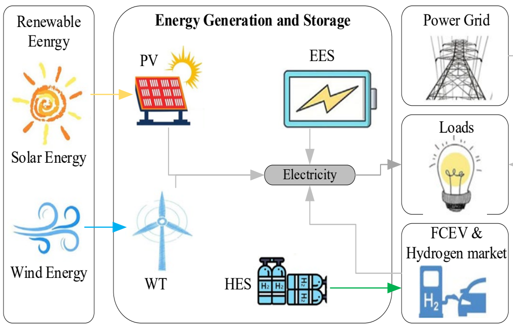

Fig 1. The proposed integrated energy system

PV, WT, FCEV, and purchase electrical energy can meet the load in the system. When the total energy generated by PV and WT is not sufficient to supply the demand, the energy shortage can be supplied by purchasing from the upstream grid or by FCEVs. In addition, to optimize operating costs and increase overall profitability, the system can purchase electricity during off-peak periods and store it using energy storage devices for use during peak periods. Also, when electricity prices are low but hydrogen prices are high, the system can purchase electricity and earn a profit by producing and selling hydrogen. The excess hydrogen produced is sold to FCEVs or in the hydrogen market. Fig. (2) illustrates the flowchart of the proposed framework.

In the modeling of IESs, accurately representing uncertainty behavior as well as managing computational burden is of great importance. The random variables governing power systems, including physical variables such as the output power of wind and solar resources and load demand, as well as economic variables such as electricity and hydrogen prices, are usually not independent and exhibit complex correlations with one another. The main reason for selecting the Copula function is that this method is capable of constructing an overall joint probability distribution by linking the marginal distributions of multiple random variables, thereby accurately describing and preserving their correlation structure and mutual dependence.

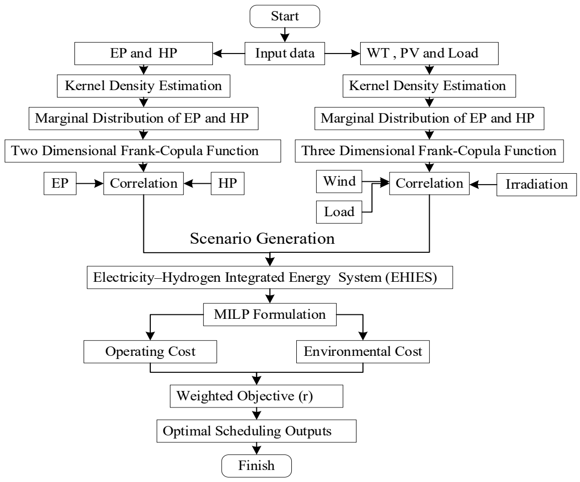

Fig 2. The flowchart of proposed framework.

In this research, the Frank-Copula family is specifically employed because it imposes minimal restrictions and requirements for describing the degree of dependence among variables and offers high flexibility in modeling different levels of correlation. Its application in the present problem is to generate initial scenarios in which the actual dependencies and behavioral patterns among REs, consumers, and market prices are properly captured.

Although generating numerous scenarios through the Copula function maximizes modeling accuracy, the large number of generated scenarios creates significant computational challenges in solving the system optimization problem. To overcome this limitation and reduce the computational burden, the K-means clustering algorithm is utilized. Due to its high efficiency and speed in grouping large datasets, K-means partitions the initial scenarios into distinct clusters based on similarities in their statistical characteristics. The centroid of each cluster is then selected as a representative scenario, and each representative scenario is assigned a probability of occurrence proportional to the number of scenarios contained in its corresponding cluster.

The marginal distribution of electricity price, hydrogen price, WT, and PV generation, as well as load energy consumption are estimated using the kernel density estimation method shown in Eq. (1). In this equation, n represents the number of samples, h is the bandwidth of the kernel density estimation, and K is the kernel density function [15].

$$\hat{f}(x) = \frac{1}{n \cdot h} \sum_{i=1}^{n} K\left(\frac{x - X_i}{h}\right) \tag{1}$$

The copula function can determine the overall distribution of variables through the marginal distribution of multivariate random variables. This function is suitable for the overall probability distribution function of PV, WT, and demand, and can accurately describe the correlation between them.

The copula function is defined according to Eq. (2). In this equation, C represents the copula function and F represents the general distribution function of n variables [15].

$$F(x_1, x_2, \dots, x_n) = C\left(\hat{f}_{x_1}(x_1), \hat{f}_{x_2}(x_2), \dots, \hat{f}_{x_n}(x_n)\right) \tag{2}$$

To describe the correlation between electricity price and hydrogen price, the two-dimensional Frank-Copula function is considered according to Eq. (3). In this equation, v_1 and v_2 represent the marginal distribution functions of electricity price and hydrogen price, respectively. Also, θ_1 represents the parameter of the two-dimensional Frank-Copula function [15].

$$C(v_1, v_2, \theta_1) = -\frac{1}{\theta_1} ln\left[1 + \frac{(e^{-\theta_1 v_1} - 1)(e^{-\theta_1 v_2} - 1)}{e^{-\theta_1} - 1}\right] \tag{3}$$

To describe the correlation between WT, PV, and loads, the three-dimensional Frank-Copula function is used according to Eq. (4). u_1, u_2, and u_3 are the marginal distribution functions of PV, WT, and demand, respectively, and θ_2 is the parameter of the three-dimensional Frank-Copula distribution [15].

$$C(u_1, u_2, u_3, \theta_2) = -\frac{1}{\theta_2} ln\left[1 + \frac{(e^{-\theta_2 u_1} - 1)(e^{-\theta_2 u_2} - 1)(e^{-\theta_2 u_3} - 1)}{(e^{-\theta_2} - 1)^2}\right] \tag{4}$$

After generating initial scenarios using copula functions, a higher number of scenarios can pose significant computational challenges in system optimization. To address this problem and reduce the computational burden, the K-means clustering algorithm has been used to reduce the number of scenarios.

Typically, price-based DRP is modeled based on the price elasticity of consumers. Price elasticity of demand is used to quantify users' response to price changes, which can well determine the extent of consumption change due to instantaneous changes in electricity prices and guide users to change their consumption behavior. Finally, as the consumer pattern changes, the peak demand of the system decreases.

In this method, the electricity consumption of users in a period depends on the price of that period and the price of other periods, which are described by the self-elasticity coefficient and the cross-elasticity coefficient, respectively. The elasticity coefficient is calculated according to Eq. (5) [15].

$$e_{ij} = \frac{\Delta q_i / q_{0i}}{\Delta p_j / p_{0j}} = \frac{(q_i - q_{0i})/q_{0i}}{(p_j - p_{0j})/p_{0j}} \tag{5}$$

In this equation, q_{0i} and q_i represent the amount of electricity consumed by consumers before and after the price change, respectively. Also, p_{j0} and p_0 represent the initial price and the price of electricity after the change, respectively. e_{ij} also represents the price elasticity of demand.

The price elasticity matrix of consumer demand, defined according to Eq. (6), is used, based on Eq. (7), to determine the final demand of consumers after applying price changes in multiple time periods. e_{ii} represents the intrinsic elasticity and e_{ij} represents the cross elasticity [15].

$$\mathbf{E} = \begin{bmatrix} e_{11} & e_{12} & \cdots & e_{1m} \\ e_{21} & e_{22} & \cdots & e_{2m} \\ \vdots & \vdots & \ddots & \vdots \\ e_{m1} & e_{m2} & \cdots & e_{mm} \end{bmatrix} \tag{6}$$

$$\begin{bmatrix} q_1 \\ q_2 \\ \vdots \\ q_m \end{bmatrix} = \begin{bmatrix} q_{01} \\ q_{02} \\ \vdots \\ q_{0m} \end{bmatrix} + \begin{bmatrix} q_{01} & 0 & \cdots & 0 \\ 0 & q_{02} & \cdots & 0 \\ \vdots & \vdots & \ddots & \vdots \\ 0 & 0 & \cdots & q_{0m} \end{bmatrix} \cdot \mathbf{E} \cdot \begin{bmatrix} \Delta p_1/p_{10} \\ \Delta p_2/p_{20} \\ \vdots \\ \Delta p_m/p_{m0} \end{bmatrix} \tag{7}$$

To generate parameters related to vehicles, the behavior of each vehicle is modeled using Eq. (8) to Eq. (10) [16].

Eq. (8) is related to determining the time of entry of each FCEV into the parking by considering the Gaussian distribution. In this regard, μ_{arv} is the average arrival time, σ_{arv} is the standard deviation of the arrival time, $t_n^{arv,min}$ is the lower limit equivalent to the minimum arrival time, and $t_n^{arv,max}$ is the maximum arrival time of the vehicle at the parking. Eq. (8) ensures that the time for FCEVs to leave the parking is greater than the time for them to enter the parking. Eq. (9) determines the time the FCEVs leave the parking, μ_{dep} and σ_{dep} are the mean and standard deviation are the time to leave the parking and the minimum time required to fill the vehicle's hydrogen tank to a certain level, respectively.

The initial charge level of the FCEVs at the time of entering the parking is also determined according to Eq. (10), where μ_{soh} is the mean and σ_{soh} standard deviation of the hydrogen level at the time of entering the parking. Also, soh_i^{min} and soh_i^{max} are the minimum and maximum possible values for the initial hydrogen level of the FCEVs, respectively [15].

$$\left\{t_i^{arv} = f_{TG}(x; \mu_{arv}, \sigma_{arv}^2), t_i^{arv} \in \left[t_i^{arv,min_i^{arv,max}}\right| t \tag{8}$$

$$t_i^{dep} = f_{TG}(x; \mu_{dep}, \sigma_{dep}^2), t_i^{dep} \in \left[max(\, t_i^{arv} + t_{ch}^{min_i^{dep,max}}\right] \tag{9}$$

$$SOH_{i,t_i^{arv}}^{EV} = f_{TG}(x; \mu_{soh}, \sigma_{soh}^2), SOH_{i,t_i^{arv}}^{EV} \in \left[soh_i^{min_i^{max}}\right] \tag{10}$$

In the proposed method, the optimal scheduling of the EHIES is modeled with the aim of reducing the cost and also reducing the environmental impacts. Accordingly, the problem is formulated and solved as a multi-objective optimization with the aim of reducing the operating cost and reducing the environmental cost. These costs are defined as follows:

- Operating costs include penalties for power outages from REs, costs of purchasing energy from the upstream grid, costs of power generation by the FCEVs, and revenue from hydrogen sales (Eq. (11)).
- Environmental cost including the cost of CO_2 emissions related to power purchased from the upstream grid, which is based on traditional sources (Eq. (12)).

$$F_1 = min\left(f_{\text{buy}} + f_{\text{dis}} - f_{FCEV} - f_{\text{sell,H}}\right) \tag{11}$$

In Eq. (11), F_1 represents the operational cost, f_{buy} represents the cost of purchasing electricity from the upstream grid, f_{dis} represents the penalty for disconnecting REs, f_{FCEV} represents the revenue from selling hydrogen to FCEVs, and $f_{sell,H}$ represents the revenue from selling the hydrogen produced. Eq. (12) presents the cost of purchasing energy from the upstream network. In this equation, the energy purchase price, and $P_{buy}(t)$ represent the energy purchased. The penalty cost of REs is calculated from Eq. (13). In this equation, ω is the penalty coefficient, $P_{W,dis}(t)$ and $P_{PV,dis}(t)$ are the shortage power of WT and PV respectively. The profit from hydrogen purchase to FCEVs is calculated from Eq. (14). α_t, $H_i^{ch}(t,i)$, and $H_i^{dch}(t,i)$ are the hydrogen price, sold hydrogen to FCEVs, and consumed hydrogen of FCEVs to generate electricity for EHIES. Eq. (15) is related to the calculation of hydrogen purchase income in another markets, which $H_{sell}(t)$ is sold hydrogen. It should be noted that the coefficient of 0.9 in Eq. (15) is considered because hydrogen is sold in other markets at a competitive price and lower than the final price for consumers [15].

$$f_{\mathrm{buy}} = \sum_{t=1}^{T} \beta_t \cdot P_{\mathrm{buy}}(t) \tag{12}$$

$$f_{\mathrm{dis}} = \omega \cdot \sum_{t=1}^{T} \left[P_{W,\mathrm{dis}}(t) + P_{PV,\mathrm{dis}}(t)\right] \tag{13}$$

$$f_{FCEV} = \sum_{t=1}^{T} \alpha_t \cdot \left[\sum_{i=1}^{NEV} H_{ev}^{ch}(t,i) - \sum_{i=1}^{NEV} H_{ev}^{dch}(t,i)\right] \tag{14}$$

$$f_{\mathrm{sell,H}} = 0.9 \cdot \sum_{t=1}^{T} \alpha_t \cdot H_{\mathrm{sell}}(t) \tag{15}$$

The second objective of optimal scheduling of the EHIES is to minimize the environmental cost of the system during the day. This objective function define as Eq. (15). In this equation, f_{co_2} is the penalty resulting from CO2 production, which is calculated based on the amount of gas produced, according to Eq. (17). F_2 illustrates the emission cost. λ represents the base price of carbon trading, I represents the length of the carbon emission allocation interval, and α represents the percentage growth of the carbon trading price. E_{IESt} represents the carbon emission trading quota, which is calculated according to Eq. (18) to Eq. (20). In these equations, E_{IESa} represents the real amount of carbon emissions produced by the system, and E_{IES} represents the total carbon emissions assigned to the system by the relevant authorities. χ_{ca} is the CO2 emissions produced by the system after purchasing a unit of electricity from the grid, and χ_c is the free carbon emission allowance that the system obtains after purchasing a unit of electricity from the grid [15].

$$F_2 = min\, f_{CO_2} \tag{16}$$

$$f_{CO_2} = \begin{cases} \lambda \cdot E_{IESt} & E_{IESt} \le I \\ \lambda \cdot I + \lambda \cdot (1+\alpha) \cdot (E_{IESt} - I) & I \le E_{IESt} \le 2I \\ \lambda \cdot (2+\alpha) \cdot I + \lambda \cdot (1+2\alpha) \cdot (E_{IESt} - 2I) & 2I \le E_{IESt} \le 3I \\ \lambda \cdot (3+3\alpha) \cdot I + \lambda \cdot (1+3\alpha) \cdot (E_{IESt} - 3I) & 3I \le E_{IESt} \le 4I \\ \lambda \cdot (4+6\alpha) \cdot I + \lambda \cdot (1+4\alpha) \cdot (E_{IESt} - 4I) & E_{IESt} \ge 4I \end{cases} \tag{17}$$

$$E_{IESt} = E_{IESa} - E_{IES} \tag{18}$$

$$E_{IESa} = \chi_{ca} \cdot P_{buy} \tag{19}$$

$$E_{IES} = \chi_c \cdot P_{buy} \tag{20}$$

Optimal system scheduling must be solved by considering various constraints of the system and its various components. These constraints are described in this section.

The amount of hydrogen energy stored in the hydrogen tank in each time period is calculated according to Eq. (21). In this equation, $E_{tan\,k}(t)$ represents the hydrogen power stored in the hydrogen tank.

$P_{tan\,k}^{ch}(t)$ and $P_{tan\,k}^{dis}(t)$ are the order of the charging and discharging of the HES. Also, $\eta_{tan\,k}^{ch}$ and $\eta_{tan\,k}^{dis}$ determine the charging and discharging efficiency of the HES.

$$\begin{aligned} E_{\mathrm{tank}}(t) = E_{\mathrm{tank}}(t-1) & \\ + \Bigg[P_{\mathrm{tank}}^{ch}(t) \cdot \eta_{\mathrm{tank}}^{ch} - \frac{P_{\mathrm{tank}}^{dis}(t)}{\eta_{\mathrm{tank}}^{dis}} & \\ - H_{\mathrm{sell}}(t) - \sum_{i=1}^{NEV} H_{ev}^{ch}(t,i) \Bigg] \cdot \Delta t & \end{aligned} \tag{21}$$

Other constraints related to the HES are modeled according to Eq. (22) to Eq. (26). Eq. (22) relates to the minimum and maximum hydrogen that can be stored in the hydrogen tank. In this equation, $E_{tan\,k}^{min}$ and $E_{tan\,k}^{max}$ are the minimum and maximum hydrogen power that can be stored in the tank, respectively. Eq. (23) and Eq. (24) are the minimum and maximum limits of the charging and discharging power of the HES, respectively, which are determined based on the nominal capacity of the EL and FC. In these equations, $P_{max}^{ch,tan\,k}$ is the maximum power consumed by the EL and $P_{max}^{dis,tan\,k}$ is the maximum power produced by the FC. I_t^{ch} and I_t^{dis} are binary variables of the charge and discharge states of the HES respectively. Eq. (25) states that at any hour, the storage device is in only one of the charging or discharging states. Eq. (26) also states that the hydrogen power level of the tank at the beginning and end of the period must be equal.

$$E_{\mathrm{tank}}^{min_{\mathrm{tank}}{}_{\mathrm{tank}}^{max}} \tag{22}$$

$$0 \le P_{\mathrm{tank}}^{ch}(t) \le I_t^{ch}(t) \cdot P_{\mathrm{tank}}^{ch,max} \tag{23}$$

$$0 \le P_{\mathrm{tank}}^{dis}(t) \le I_t^{dis}(t) \cdot P_{\mathrm{tank}}^{dis,max} \tag{24}$$

$$0 \le I_t^{ch}(t) + I_t^{dis}(t) \le 1 \tag{25}$$

$$E_{\mathrm{tank}}(0) = E_{\mathrm{tank}}(T) \tag{26}$$

The maximum hydrogen that can be sold to hydrogen consumers is also limited, which is defined as Eq. (27). $H_{sell,max}$ is the maximum capability for selling hydrogen.

$$0 \le H_{\mathrm{sell}}(t) \le H_{\mathrm{sell},max} \tag{27}$$

The model and limitations of the EES are taken from Ref [17] and [18], which is similar to the HES, which is not stated for brevity.

As mentioned, the system has a parking for FCEVs that charge their hydrogen tanks. The hydrogen level of the FCEVs while in the parking is determined according to Eq. (28).

$$\begin{aligned} SOH(t,i) &= SOH(t-1,i) \\ &+ [H_{ev}^{ch}(t,i) - H_{ev}^{dch}(t,i)] \cdot \Delta t \end{aligned} \tag{28}$$

According to Eq. (28), the hydrogen level of the vehicle tank is determined based on the previous hydrogen level and the amount of hydrogen charging and discharging. Other constraints related to FCEVs are defined according to Eq. (29)

to Eq. (31). Eq. (36) states that the hydrogen level of the FCEV must be maintained at a certain level while in the parking. Eq. (37) is related to the limit on the maximum power injected by FCEV into the network, and Eq. (38) also states that the hydrogen level of FCEV at the time of leaving the parking must be at least equal to the level set by the vehicle owner, i.e $SOH^{dep}(i)$.

$$SOHmax_{min} \tag{29}$$

$$0 \leq P_{ev}^{dis}(t,i) \leq P_{ev}^{dis,max} \tag{30}$$

$$SOH(t,i)|t = tdep \geq SOH^{dep}(i) \tag{31}$$

In each time period, the amount of electrical energy produced and consumed in the system must be balanced. This constraint is expressed as Eq. (32). In this equation, $P_{load}(t)$ is the electrical energy demand from system consumers. Also, P_{PV} and P_W are the solar and wind energy used.

$$\begin{aligned} P_{\text{load}}(t) = P_{PV}(t) + P_W(t) + P_{\text{bat}}^{dis}(t) - P_{\text{bat}}^{ch}(t) \\ + P_{\text{tank}}^{dis}(t) - P_{\text{tank}}^{ch}(t) + P_{\text{buy}}(t) \\ + \sum_{i=1}^{NEV} \frac{H_{ev}^{dch}(t,i)}{\eta_i^{dch}} \end{aligned} \tag{32}$$

The maximum usable power of solar and wind resources is obtained according to Eq. (33) and Eq. (34), respectively. P_{PV}^{P} and P_W^P are predicted PV and WT power generation, respectively [15].

$$0 \leq P_{PV}(t) \leq P_{PV}^{p} \tag{33}$$

$$0 \leq P_W(t) \leq P_W^{p} \tag{34}$$

Based on the used PV and WT and the amount of their generated power, the power cut of PV and WT is calculated as Eq. (42) and Eq. (43).

$$P_{PV,\text{dis}}(t) = P_{PV}^{p}(t) - P_{PV}(t) \tag{35}$$

$$P_{W,\text{dis}}(t) = P_W^{p}(t) - P_W(t) \tag{36}$$

The maximum power that can be purchased from the upstream network is also a limitation, which is formulated as Eq. (37).

$$0 \leq P_{\text{buy}} \leq P_{\text{buy}}^{max} \tag{37}$$

3 Simulation and Numerical Results

In this section, the performance of the proposed model for scheduling an EHIES is evaluated by considering different cases. First, the effect of considering price-based DRP is examined. Next, the effect of seasonal conditions and the effect of the weighting coefficient on the objective function are studied. Finally, the system conditions have been evaluated in terms of using FCEVs to inject electric power into the system. Table. 1 provide input data for storage systems.

In order to evaluate the impact of DRP, the scheduling problem is solved by considering a weighting factor of 0.7 in the objective function for all three seasons. The problem has been solved in two cases, with DRP and without DRP. The numerical results obtained for these cases in each season are given in Table (2). Based on the results presented in Table (2), it can be seen that considering demand response leads to a simultaneous reduction in the peak-valley demand difference as well as the system operating cost in all seasons of the year.

Table 1. Parameters of Energy Storage.

System	Parameters	Value
Hydrogen storage	Hydrogen storage tank capacity (kWh)	500
	Maximum charging power (kW)	100
	Maximum discharging power (kW)	100
	Maximum hydrogen selling power (kW)	50
	Charging efficiency	0.8
	Discharging efficiency	0.8
	Upper limit of transmission power (kW)	50
Battery storage	Battery capacity (kWh)	500
	Maximum charging power (kW)	100
	Maximum discharging power (kW)	100
	SOC_min	0.2
	SOC_max	0.8
	Self-discharging rate (/day)	0.46%
	Charging efficiency	0.9
	Discharging efficiency	0.9
	The maximum number of charging and discharging times in the transition season	12
	The maximum number of charging and discharging times in summer and winter	10

Table 2. Numerical results obtained from simulation for R = 0.7 under two different cases.

Case No.	Season	Operation Cost (USD/day)	Environmental Cost (USD/day)	Peak–Valley Demand Difference (kW)
Case 1: Without considering DR	Spring & Autumn	96.17	172.71	83.42
	Summer	99.24	187.4	99.94
	Winter	262.2	316.77	111.73
Case 2: Considering DR	Spring & Autumn	86.29	167.66	69.57
	Summer	92.36	184.59	83.36
	Winter	237.84	302.58	86.49

The system's electrical energy demand before and after applying DR for each season is shown in Fig. (3) to Fig. (5). These three graphs show that after implementing the DRP, the system's load profile (red curve) became more balanced and fluctuations decreased. As a result, the DRP improved network stability and reduced peak demand during high-load hours.

In Case 2, the peak and off-peak demand difference for the mid-season, summer, and winter seasons has decreased by 16.6%, 16.59%, and 22.5%, respectively, compared to Case 1 (without DRP), which is a result of consumer participation in the DR program. Also, the system operating cost in Case 2 for the mid-season, summer, and winter seasons has decreased by 10.2%, 7%, and 9.3%, respectively, compared to Case 1, which is a significant saving. In addition, the results show that consumer participation in DRP in the mid-season, summer, and winter seasons has reduced the environmental cost by 3, 1.5%, and 4.48%, respectively.

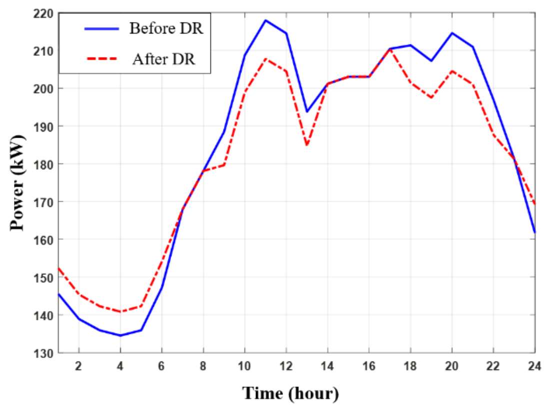

Fig. 3: Demand of electric energy consumers before and after applying DR in the middle seasons.

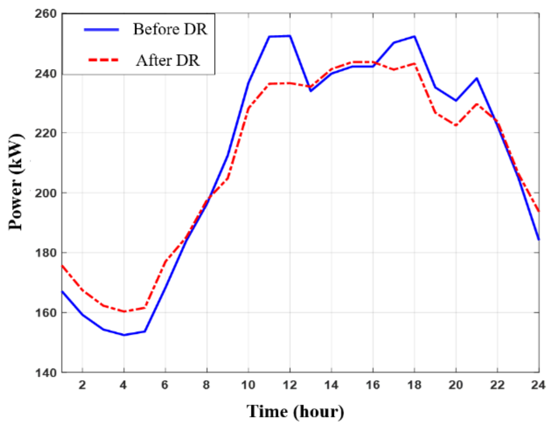

Fig. 4: Demand of electrical energy consumers before and after DR implementation in the summer.

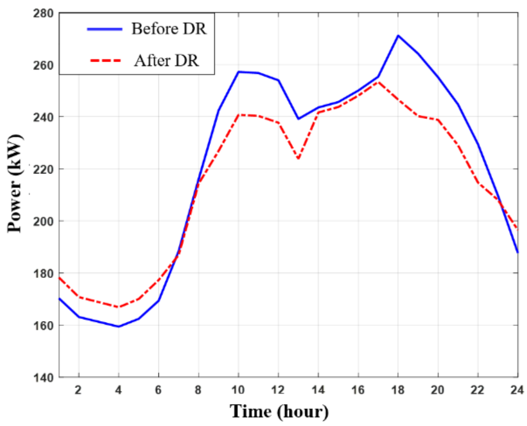

Fig. 5: Demand of electric energy consumers before and after applying DR in the winter.

In this section, the results obtained for optimal scheduling considering DRP and also for the weighting factor r=0.7 are examined.

Fig. (6) to Fig. (8) show the power generated and consumed by each part of the system, and Fig. (9) also shows the power purchased from the upstream network for each season. Fig. (6) shows that generation generally tracks demand with moderate variation; for example, during one of the mid-day intervals, total production rises to roughly match the increased consumption level. A noticeable dip later in the chart corresponds to reduced demand, where production similarly drops by several kilowatts to maintain balance.

Based on Fig. (9) to Fig. (10), it can be seen that in all cases, the balance of electrical energy produced and consumed in the EHIES is maintained. It is also known that EES and HES are charged during off-peak hours when the price of purchasing electricity from the grid is low, by purchasing energy from the grid or using RESs, and are discharged during peak demand hours when the price of energy is higher, meeting part of consumer demand. This not only reduces the cost of operating the system, but also makes it possible to use the power generated by RESs at other times.

According to Fig. (9), the power purchased from the upstream network was close to each other in the mid-season and summer season, but this amount increased significantly in the winter season. The reason for this increase is the decrease in the production capacity of RES in the winter, which increases the energy system's dependence on the upstream network. Based on the results of the previous section, it was found that the operating cost and environmental cost in winter are very high compared to the other two seasons, which is due to the high share of electricity purchased from the grid in this season.

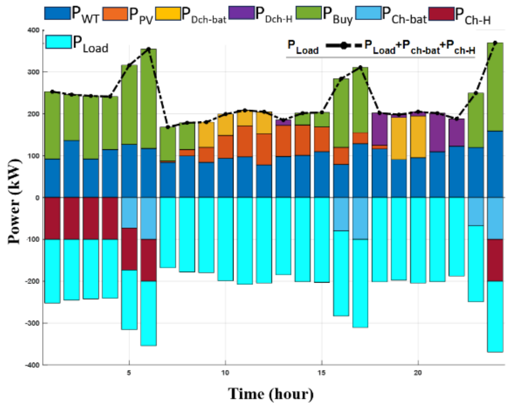

Fig. 6: Production and consumption power in different parts of the system for the middle seasons.

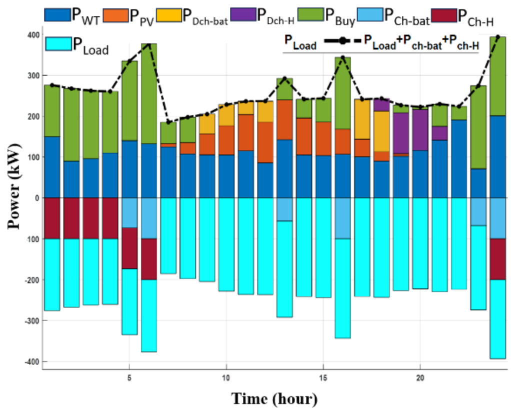

Fig. 7: Production and consumption power in different parts of the system for the summer.

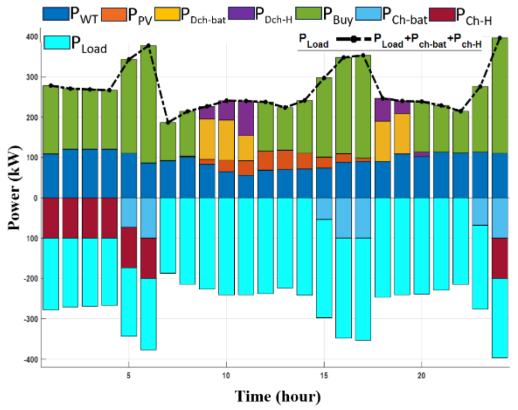

Fig. 8: Production and consumption power in different parts of the system for the winter.

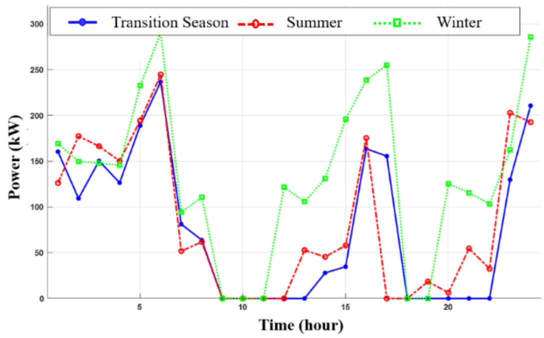

Fig. 9: Power purchased from the grid for each season

Fig. (10) and Fig. (11) show the level of stored energy and the charging/discharging power for the EES and HES, respectively. Fig. (12) shows the hydrogen power sold. According to the results presented, in the initial hours of the day (1-7 am) when the energy price is very low, the system purchases energy from the grid, converts it into hydrogen and sell. In the early morning hours, due to low consumer demand, the price of purchasing energy from the grid is low, so the system has earned income by converting it into hydrogen and selling the hydrogen.

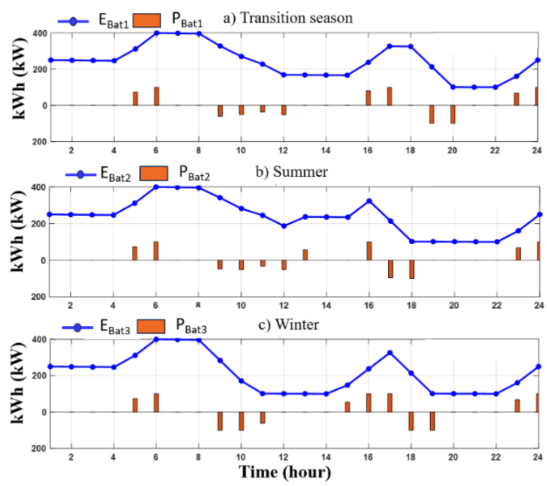

Fig. 10: Stored energy and charge/discharge power of the EES per season.

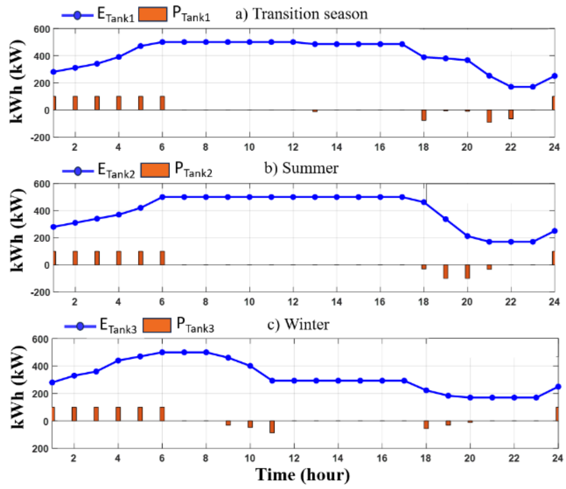

Fig. 11: Stored energy and charge/discharge power and sold hydrogen storage device per season.

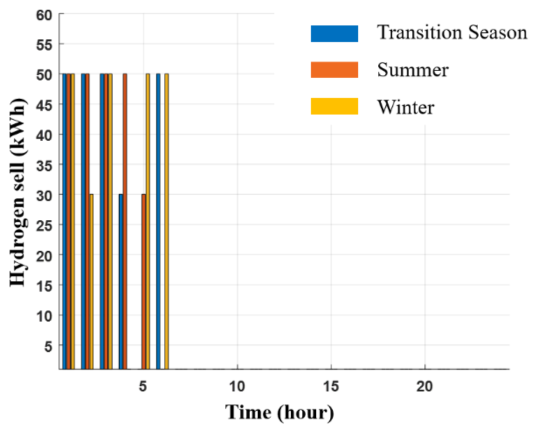

Fig. 12: Hydrogen sold to FCEVs and other markets in each season.

Also, due to the limited sale of hydrogen, in the early morning hours, the amount of hydrogen produced is greater than the amount sold, and the excess amount sold is stored in the hydrogen tank and converted back into electrical energy during peak hours to meet consumer demand.

In order to evaluate the impact of the objective function weighting factor on economic efficiency and environmental cost, in this section the problem is solved by considering different values for r.

In Table. (3), the economic cost, environmental cost and the sum of both costs are presented based on the value of r. According to this table, it is observed that in all three seasons, the lowest cost is related to the value of r = 0.5, which has created a compromise between economic cost and environmental cost. Based on Fig. (13) to Fig. (15), it is observed that for values of 0.4 to 0.6, economic and environmental cost have appropriate values and the decision maker can choose the optimal response from among the different responses based on the priority of exploitation.

Table 3. Results of optimal system scheduling for different values of the objective function weighting coefficient in different seasons.

winter			summer			Transition season			r
F_1+F_2	F_2	F_1	F_1+F_2	F_2	F_1	F_1+F_2	F_2	F_1	
550.4	246.2	304.2	275.1	133.1	142	251.85	116.6	135.25	0.1
544.8	247.4	297.4	270	134.2	135.8	247.8	117.4	130.4	0.2
534.2	251.6	282.6	264.7	137.2	127.5	241.3	120.7	120.6	0.4
526.5	262.5	264	264	137.8	126.2	241.2	120.9	120.3	0.5
524.8	270	254.8	263.9	138.9	125	240.1	135.9	104.21	0.5
524.9	271.9	253	264.8	155.4	109.4	240.6	138.8	101.8	0.6
540.4	302.6	237.8	276.9	184.6	92.3	253.9	167.7	86.3	0.8
540.4	302.6	237.8	293.7	210.8	82.9	273.3	194	79.3	0.8
540.4	302.6	237.8	360.9	291.1	69.8	334.2	262.5	71.7	0.9

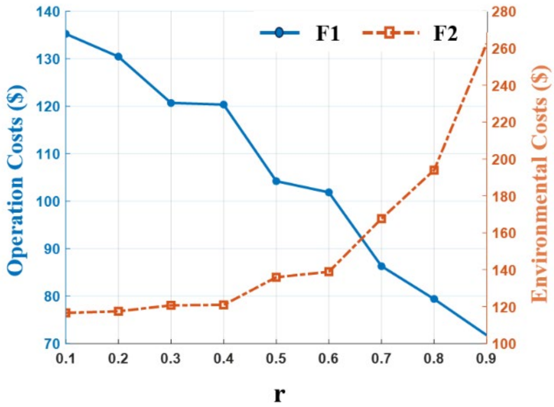

Fig. 13: Economic and environmental costs based on the value of the weighting factor r in middle seasons.

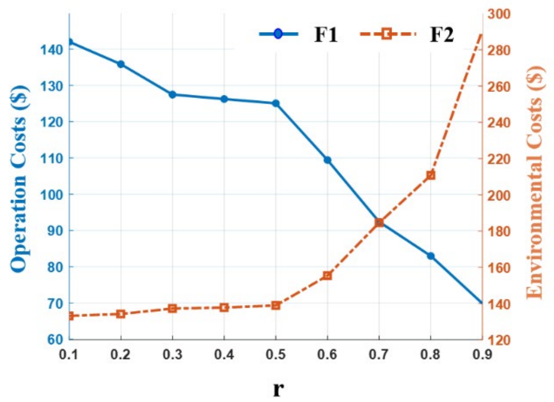

Fig. 14: Economic and environmental costs based on the value of the weighting factor r in the summer.

Given that the installation of a hydrogen tank and battery has a high initial cost, it is assumed in the following that the system does not have a battery and a hydrogen tank. On the other hand, purchasing electrical energy from the upstream grid is cheaper than producing electrical energy through hydrogen from FCEV vehicles. Therefore, the limit on purchasing electrical energy from the upstream grid is also reduced to 150 kW. For this condition, the hydrogen delivered to the FCEVs in each season is shown in Fig. (16).

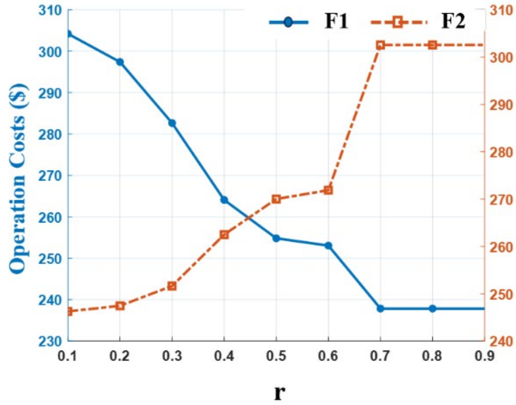

Fig. 15: Economic and environmental costs based on the value of the weighting factor r in winter.

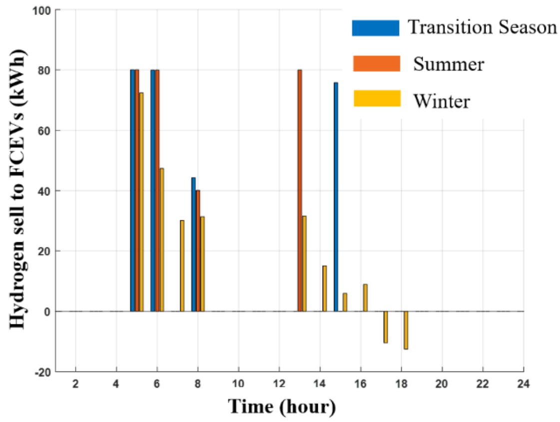

Fig. 15: Hydrogen sold to FCEVs per season.

According to Fig. (16), it is observed that most of the hydrogen delivered to the FCEVs was done in the early morning hours when the system energy demand was lower. It is also observed that at 5:00 PM and 6:00 PM in the winter, the amount of hydrogen delivered to the vehicles became negative. Therefore, during these hours, the hydrogen stored in the FCEV vehicle tank was used to produce and inject electrical energy into the EHIES system. The simulation results show that at 5:00 PM and 6:00 PM in the winter, due to the low production of wind and solar resources, it is not possible to supply the EHIES system load and the hydrogen required by the FCEV vehicles without discharging the FCEV vehicles.

At 17:00 and 18:00, the system operator generated and injected electrical energy into the system using hydrogen stored in the FCEV vehicle tank. As a result, the system's energy requirements were reliably met and there was no need to cut off the load. Therefore, these results prove that the use of V2G technology in FCEV vehicles provides a more reliable supply of energy to the system and improves system reliability. In addition, with the development of hydrogen-to-electricity technologies, it is predicted that the efficiency of converting hydrogen energy into electrical energy will increase in the coming years. Therefore, V2G technology will also become more important in hydrogen vehicles.

4 Conclusion

This study presented an optimal day-ahead scheduling model for an electricity-hydrogen Integrated Energy System (IES), addressing correlated uncertainties, demand response (DR), and hydrogen vehicle fleets. Simulation results confirmed that modeling uncertainties using Copula functions and applying k-means clustering for scenario reduction provided realistic decision-making capabilities while ensuring the computational feasibility of the MILP model.

The implementation of price-based DR proved critical for enhancing economic and environmental performance. Results indicated that DR significantly smoothed the load profile, reducing the peak-to-valley difference by 16.6%, 16.59%, and 22.5% in transition season, summer, and winter, respectively. Consequently, operational costs decreased by 10.2%, 7%, and 9.3% across these seasons. Furthermore, consumer participation led to a reduction in environmental costs by 3%, 1.5%, and 4.48%, demonstrating the efficacy of DR in lowering emissions.

Multi-objective analysis revealed that a weighting factor between 0.4 and 0.6 establishes an optimal trade-off between economic and environmental goals. Furthermore, the study provided a detailed assessment of Fuel Cell Electric Vehicles (FCEVs) equipped with Vehicle-to-Grid (V2G) technology. The results showed that FCEVs can go beyond passive consumption to act as active storage units. Specifically, under critical operating conditions, the V2G capability enabled the fleet to function as a vital emergency backup resource, significantly bolstering the reliability and resilience of the integrated energy system.

Ultimately, integrating DR, hydrogen storage, and accurate uncertainty modeling offers a sustainable pathway for high renewable penetration and low-carbon energy system development.

One of the limitations of this study is the omission of the power grid and hydrogen network models, which would make the proposed framework closer to real-world conditions. Therefore, for future work, it is recommended to incorporate the models and constraints of the power and hydrogen networks to enhance the comprehensiveness of the proposed model.

Disclosure of Potential Conflicts of Interest

The Authors declare that there is no conflict of interest

Reference

[1] H. Zhu et al., “A review of integrated energy system modeling and operation,” *Applied Energy*, vol. 400, p. 126572, Dec. 2025, doi: 10.1016/j.apenergy.2025.126572.

[2] F. Ruiming, “Multi-objective optimized operation of integrated energy system with hydrogen storage,” *International Journal of Hydrogen Energy*, vol. 44, no. 56, pp. 29409–29417, Nov. 2019, doi: 10.1016/j.ijhydene.2019.02.168.

[3] R. Fang, “Life cycle cost assessment of wind power–hydrogen coupled integrated energy system,” *International Journal of Hydrogen Energy*, vol. 44, no. 56, pp. 29399–29408, Nov. 2019, doi: 10.1016/j.ijhydene.2019.03.192.

[4] G. Pan, W. Gu, Y. Lu, H. Qiu, S. Lu, and S. Yao, “Optimal Planning for Electricity-Hydrogen Integrated Energy System Considering Power to Hydrogen and Heat and Seasonal Storage,” *IEEE Trans. Sustain. Energy*, vol. 11, no. 4, pp. 2662–2676, Oct. 2020, doi: 10.1109/tste.2020.2970078.

[5] G. Pan, W. Gu, H. Qiu, Y. Lu, S. Zhou, and Z. Wu, “Bi-level mixed-integer planning for electricity-hydrogen integrated energy system considering levelized cost of hydrogen,” *Applied Energy*, vol. 270, p. 115176, Jul. 2020, doi: 10.1016/j.apenergy.2020.115176.

[6] P. Ge, Q. Hu, Q. Wu, X. Dou, Z. Wu, and Y. Ding, “Increasing operational flexibility of integrated energy systems by introducing power to hydrogen,” *IET Renewable Power Gen*, vol. 14, no. 3, pp. 372–380, Jan. 2020, doi: 10.1049/iet-rpg.2019.0663.

[7] A. E. H. Berjawi, S. L. Walker, C. Patsios, and S. H. R. Hosseini, “An evaluation framework for future integrated energy systems: A whole energy systems approach,” *Renewable and Sustainable Energy Reviews*, vol. 145, p. 111163, Jul. 2021, doi: 10.1016/j.rser.2021.111163.

[8] D. Zhou et al., “Modeling and simulation of the hydrogen blended gas-electricity integrated energy system and influence analysis of hydrogen blending modes,” *Energy*, vol. 239, p. 121629, Jan. 2022, doi: 10.1016/j.energy.2021.121629.

[9] X. Liu, “Optimal scheduling strategy of electricity-heat-hydrogen integrated energy system under different operating modes,” *Intl J of Energy Research*, vol. 46, no. 9, pp. 12901–12925, May 2022, doi: 10.1002/er.8063.

[10] J. Zhou et al., “Operation optimization for gas-electric integrated energy system with hydrogen storage module,” *International Journal of Hydrogen Energy*, vol. 47, no. 86, pp. 36622–36639, Oct. 2022, doi: 10.1016/j.ijhydene.2022.08.224.

[11] Z. Chen, X. Yiliang, Z. Hongxia, G. Yujie, and Z. Xiongwen, “Optimal design and performance assessment for a solar powered electricity, heating and hydrogen integrated energy system,” *Energy*, vol. 262, p. 125453, Jan. 2023, doi: 10.1016/j.energy.2022.125453.

[12] S. Ahhmadi and M. Setayesh Nazar, “Economic Operation of Multi-Carrier Microgrids Considering Energy Markets and Renewable Electricity Production,” *Power, Control, and Data Processing Systems*, vol. 2, no. 2, Jun. 2025, doi: 10.30511/pcdp.2025.2060622.1025.

[13] Q. Wu, M. Chen, H. Ren, Q. Li, and W. Gao, “Collaborative modeling and optimization of energy hubs and multi-energy network considering hydrogen energy,” *Renewable Energy*, vol. 227, p. 120489, Jun. 2024, doi: 10.1016/j.renene.2024.120489.

[14] N. Liu, K. Zhang, and K. Zhang, “Coordinated configuration of hybrid energy storage for electricity-hydrogen integrated energy system,” *Journal of Energy Storage*, vol. 95, p. 112590, Aug. 2024, doi: 10.1016/j.est.2024.112590.

[15] P. Chang, C. Li, Q. Zhu, T. Zhu, and J. Shi, “Optimal scheduling of electricity and hydrogen integrated energy system considering multiple uncertainties,” *iScience*, vol. 27, no. 5, p. 109654, May 2024, doi: 10.1016/j.isci.2024.109654.

[16] E. Heydarian-Forushani, M. E. H. Golshan, and M. Shafie-khah, “Flexible interaction of plug-in electric vehicle parking lots for efficient wind integration,” *Applied Energy*, vol. 179, pp. 338–349, Oct. 2016, *doi: 10.1016/j.apenergy.2016.06.145*.

[17] S. Ahmadi and M. S. Nazar, “Stochastic Day-Ahead Economic Operation Scheduling of Multi-Carrier Microgrids Considering Energy Markets and Demand Response,” *2025 12th Iranian Conference on Renewable Energies and Distributed Generation (ICREDG). IEEE*, pp. 1–6, Feb. 26, 2025. doi: 10.1109/icredg66184.2025.10966103.

[18] S. Ahmadi, S. Lotfi, and M. S. Nazar, “Simultaneous scheduling of electricity and gas network operations considering energy markets and renewable-source uncertainty,” *2025 15th Smart Grid Conference (SGC). IEEE*, pp. 1–6, Dec. 02, 2025. doi: 10.1109/sgc69320.2025.11372329.